Bacterial outer membrane vesicles as cationic dye carriers for optoacoustics-guided phototherapy of cancer

Nian Liu[1,2,3†], Vipul Gujrati[1,2*†], Juan Pablo Fuenzalida Werner[2], Kanuj Mishra[2], Pia Anzenhofer[2], Andre C. Stiel[2], Gabriele Mettenleiter[4], Annette Feuchtinger[4], Axel Walch[4] and Vasilis Ntziachristos[1,2,5,6*]

†Nian Liu and Vipul Gujrati contributed equally.

*Correspondence:
vipul.gujrati@tum.de;
bioimaging.translatum@tum.de

[1] Chair of Biological Imaging at the Central Institute for Translational Cancer Research (TranslaTUM), School of Medicine, Technical University of Munich, Munich, Germany
[2] Institute of Biological and Medical Imaging, Helmholtz Zentrum München, Neuherberg, Germany
[3] PET Center, Department of Nuclear Medicine, The First Affiliated Hospital, Zhejiang University School of Medicine, Hangzhou 310003, China
[4] Research Unit Analytical Pathology, Helmholtz Zentrum München (GmbH), Neuherberg, Germany
[5] Munich Institute of Robotics and Machine Intelligence, Technical University of Munich, Munich, Germany
[6] DZHK (German Centre for Cardiovascular Research), Partner Site Munich Heart Alliance, Munich, Germany

Abstract

Background: Cationic dyes are widely used as biomarkers for optical imaging. However, most of these are hydrophobic and cannot be employed in vivo without chemical conjugation or modification. Herein, we report for the first time the use of bacterial outer membrane vesicles (OMVs) as nanocarriers of cationic dyes for cancer theranostics.

Results: We demonstrate that cationic dyes (IR780, Cy7, and Cy7.5) form stable complexes with negatively charged bacterial-OMVs, improving the dyes' in vivo circulation and optoacoustic properties. Such OMV-Dye complexes are biodegradable and safe for in vivo applications. Importantly, this method of cationic dye loading is faster and easier than synthetic chemistry approaches, and the efficient tumor accumulation of OMV-Dyes enables sensitive tumor detection using optoacoustic technology. As a proof-of-concept, we generated OMV-IR780 for optoacoustics-guided in vivo tumor phototherapy in a mouse model.

Conclusions: Our results demonstrate cationic dye-bound OMVs as promising novel nanoagents for tumor theranostics.

Keywords: Bacterial outer membrane vesicles, Cationic dyes, Electrostatic interaction, Optoacoustics, Phototherapy

Background

Organic dyes are highly promising candidates for preclinical and clinical optical and optoacoustic imaging applications because of their favorable optical properties, biocompatibility, and low toxicity (Li et al. 2021; Liu et al. 2019a, b). In particular, cationic dyes enable specific labeling and optical detection through their interaction with negatively charged biological components (e.g. DNA (Kotras et al. 2019), eukaryotic and prokaryotic cells (George et al. 2009; Li et al. 2015)). However, the non-specific electrostatic interactions of cationic dyes can adversely affect other negatively charged components (e.g. red blood cell aggregation) (He et al. 2019). Additionally, most of these dyes have

poor solubility in water and therefore cannot be used in vivo without any chemical conjugation or modification (Liu et al. 2021a, b, c).

A variety of nano-formulations have been proposed to enhance the stability and bioavailability of cationic dyes (Wang and Niu 2021; Cai et al. 2018; Svechkarev et al. 2019). Liposomes, micelles and polymers are biocompatible nanocarriers that can improve the pharmacokinetics of dyes (Nunes et al. 2018; Beziere et al. 2015; Kuang et al. 2017; Leriche et al. 2019). Inorganic particles are also used in dye delivery. However, inorganic nano-formulations exhibit poor biocompatibility and most synthetic agents must be chemically modified and conjugated to develop effective nanoformulations for in vivo applications (Wang and Niu 2021). Protein-based nanocarriers (e.g. human serum albumin, transferrin) are amenable to clinical translation because of their excellent biodegradability, biocompatibility, and functionalization capability (Wang et al. 2016; Jiang et al. 2015). But these types of nanocarriers usually need chemical modification to expose the hydrophobic parts to enable hydrophobic interactions.

Outer Membrane Vesicles are bilayered spherical (50–300 nm) nano-structures released from various Gram-negative bacterial strains during normal growth (Li and Liu 2020). OMVs naturally carry cell-derived cargos, including lipopolysaccharides (LPS), phospholipids, peptidoglycan, proteins (periplasmic, cytoplasmic, and membrane-bound), nucleic acids (DNA, RNA), and signaling molecules, and effectively transfer the bio-molecules to the host cell (Furuyama and Sircili 2021). Exploring the natural cargo-delivery properties of OMVs, a series of therapeutic drugs (siRNA, microRNA, biopolymers, and proteins) were delivered by encapsulating drugs in the membrane, lumen, or on the surface of OMVs (Furuyama and Sircili 2021; Qing et al. 2019; Gujrati et al. 2014, 2019). As a nanocarrier, OMVs offers several distinct advantages: they have a rigid lipoprotein membrane, which imparts stability and reduces leakage in the systemic circulation; they are acellular therefore non-replicating, which reduces the chance of infections; they can be used in vivo in very small quantities (Schwechheimer and Kuehn 2015); they exhibit strong electrostatic interactions with cationic conjugated polymers due to the negative charge of membrane and LPS, which enhances their surface binding (He et al. 2019; Avila et al. 2021). OMVs can be prepared from genetically engineered bacterial strains with substantially reduced pathogenicity, and cytotoxicity; finally, OMVs are biodegradable and can be produced in large scale by previously optimized fermentation and purification procedures (Gujrati et al. 2014, 2019).

We, therefore, hypothesized that bacterial OMVs can be used as carriers of cationic dyes for optoacoustic image-guided phototherapy (Fig. 1). To this end, we employed OMVs from an engineered strain of bacteria with reduced endotoxicity (Gujrati et al. 2014, 2019) and explored their ability to bind various near-infrared (NIR) absorbing cationic dyes (IR780, Cy7, and Cy7.5). Furthermore, the cationic dyes and OMV complexes (OMV-Dyes) were evaluated based on their zeta potential, nano-size, stability, and optoacoustic performance in tissue-mimicking agar phantoms and mouse tumor models. Finally, as a proof-of-concept, we employed the readily available IR780 dye to generate OMV-IR780 complexes for optoacoustics-guided in vivo phototherapy (photodynamic therapy and photothermal therapy) in a mouse tumor model. This study establishes OMV-Dye complexes as efficient nanocarriers of cationic dyes for tumor theranostics applications.
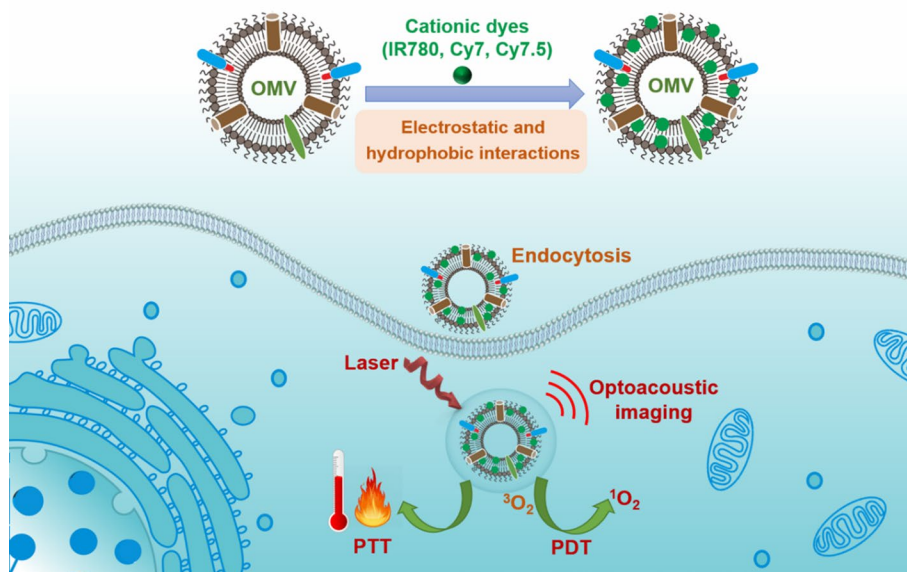
Fig. 1 Schematic representation of OMV-Dye complex generation for optoacoustic image-guided phototherapy, where the cationic dye encapsulated in and over the phospholipid bilayer
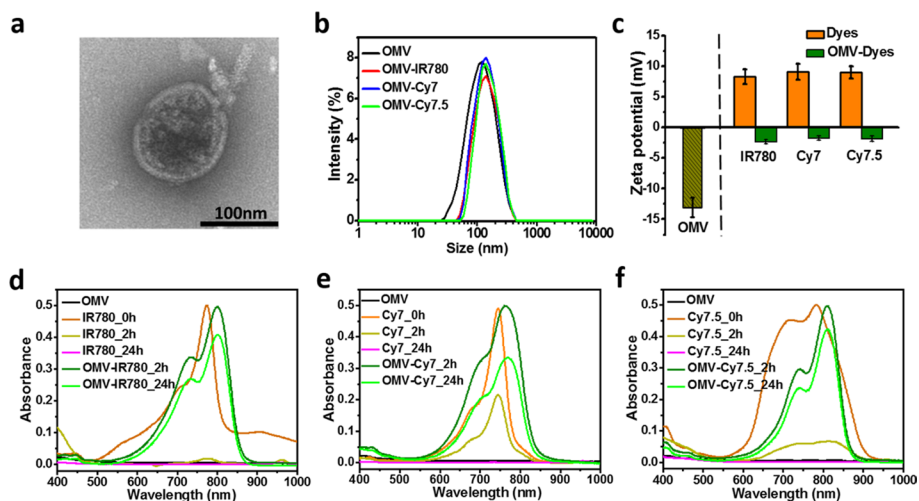
Fig. 2 Development and characterization of OMV-Dye complex. **a** Transmission electron microscopy image of OMV. **b** Dynamic light scattering profile of OMV and OMV-Dye complexes. **c** Zeta potential of OMV, free dyes (IR780, Cy7, Cy7.5), and OMV-Dye complexes. **d**, **e**, **f** The absorption spectrum of OMV, free dyes (IR780, Cy7, Cy7.5) and OMV-Dye complexes until 24 h

Results

Formulation and characterization of OMV-Dyes

A genetic mutation in the bacterial msbB gene results in the loss of endotoxic activity of lipopolysaccharide, and low immunogenic potential and cytotoxicity. Therefore, in the current study, OMVs were produced from the msbB mutant E. coli K-12 W3110 strain (Gujrati et al. 2019; Gujrati and Jon 2014). As OMVs have a negative charge (zeta potential: ~ − 13 mV; Fig. 2c) with a 20–300 nm size range (Fig. 2a), we chose several

cationic dyes with positive charge (IR780, Cy7, and Cy7.5) and anionic dyes with negative charge (ICG, CR780) to explore the binding capability of OMVs, with their detailed structures shown in Additional file 1: Fig. S1. Only the cationic IR780, Cy7, and Cy7.5 dyes bind with OMVs to form stable complexes that appear as dark precipitates (after mixing, repeated centrifugation and washing steps detailed in the methods). The anionic dyes, ICG and CR780, do not interact with the OMVs, and are removed in washing steps. When a control containing only free cationic dye in phosphate buffer (PBS) was subjected to similar conditions of repeated centrifugation and washing, dye aggregates were observed after the 1st round of centrifugation. However, after resuspension of the dye aggregates, subsequent centrifugation steps did not yield further dye aggregates and the free dyes were removed by the washing steps. We also evaluated the dyes lipophilicity by using the octanol–water partition coefficient (log P) to determine the likelihood of enhanced interaction between dye and OMV lipid membranes. The experimental log P values of IR780, Cy7, and Cy7.5 dyes are 0.8, 0.6, and 0.85 respectively, which indicate that the IR780 and Cy7.5 are the most lipophilic that might also contribute to OMV membrane labelling. We subsequently evaluated the OMV-Dye complexes in solution by dynamic light scattering (DLS), with the OMV-Dyes showing a similar size distribution as empty OMVs (Fig. 2b). The loading efficiency of IR780, Cy7, and Cy7.5 into OMVs were 7.89%, 6.95%, and 8.08%, respectively. We next measured the zeta potential of each complex to determine whether the electrostatic interactions play an essential role in the binding ability of the OMVs. Figure 2c shows that the formed OMV-Dye complexes became weakly electronegative when negatively charged OMVs bonded with positively charged cationic dyes. Next, we tested the stability of OMV-Dyes by comparing their absorption spectra with free dyes (IR780, Cy7, and Cy7.5). Figure 2d–f shows that only OMV had no NIR absorption and all three types of OMV-Dye complex in PBS remained stable over the tested period of 24 h, while the absorbance of free dyes substantially dropped, which may be due to dyes structural instability in aqueous media.

Optoacoustic imaging with OMV-Dyes in vitro and in vivo

To explore the potential optoacoustic applications of OMV-Dyes, we first evaluated their optoacoustic properties using tissue-mimicking agar phantoms. Figure 3a shows that strong optoacoustic signals were generated from OMV-Dyes (IR780, Cy7, and Cy7.5), but not from empty OMVs. Figure 3b demonstrates the corrected optoacoustic spectra of OMV-IR780, OMV-Cy7, and OMV-Cy7.5 at their specific absorption peaks (800 nm, 760 nm, and 810 nm, respectively), which were consistent with their absorption spectra (Fuenzalida Werner et al. 2020). Fig. S2 shows the plot of optoacoustic signal intensity at different concentrations of OMV-Dyes. Considering the promising optoacoustic properties of these OMV-Dyes, we generated 4T1 tumor mouse models to investigate the possibility of using OMV-Dyes for tumor detection in vivo. Figure 3c displays representative unmixed multispectral optoacoustic tomography (MSOT) images of 4T1 tumor-bearing mice at 0 h (pre-injection) and at 6 h and 24 h after intravenous injection of OMV-Dyes. The green signals depict the unmixed OMV-Dye signal in the tumor regions. As observed from the optoacoustic signal strengths at the various time points, all three tested OMV-Dyes reached the tumor region gradually, with the more prolonged accumulation until 24 h because of the enhanced permeability and retention effect (Fig. 3d).
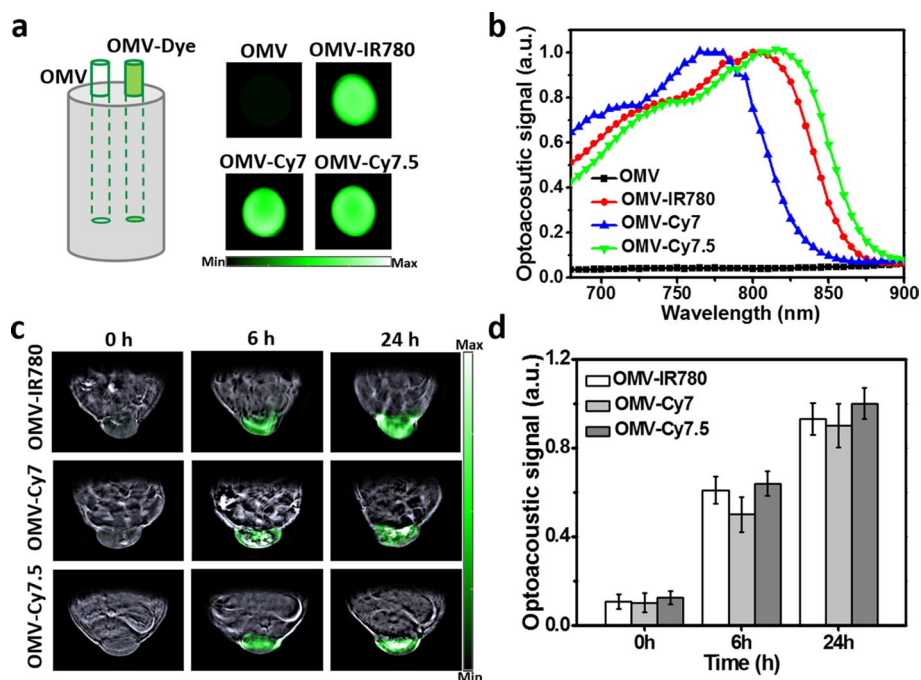
Fig. 3 Optoacoustic imaging with OMV-Dyes in vitro and in vivo. **a**, **b** Optoacoustic phantom imaging of OMV, OMV-IR780, OMV-Cy7, and OMV-Cy7.5 and their optoacoustic spectra. **c** Representative unmixed MSOT images of a 4T1 subcutaneous tumor mouse model intravenously injected with 100 μL of OMV-IR780, OMV-Cy7, and OMV-Cy7.5 (~ 100 μg OMVs), (n = 5). The green color shows an unmixed OMV-dye signal in the tumor region. **d** Quantification of panel-c: OMV-IR780, OMV-Cy7, and OMV-Cy7.5 concentrations in the tumor region measured over time

The animals injected with free OMVs did not show significant differences in the optoacoustic signal before and after injection and free IR780 dyes could not retain longer as that of OMV-IR780 in the tumor (Additional file 1: Fig. S3 and Fig. 3c). After 24 h, the major organs (kidney, heart, spleen, liver) and tumors from animals treated with the three types of OMV-Dyes were isolated and subjected to optoacoustic measurements to evaluate their biodistribution. Fig. S4 shows optoacoustic coronal plane images and corresponding optoacoustic intensities of the various organs, where a higher accumulation was seen in the liver, and a lower uptake was seen in the kidney, spleen, tumor, and heart.

Photothermal and photodynamic effects of OMV-IR780 in vitro

IR780, Cy7, and Cy7.5 are cyanine dyes that exhibit photothermal and photodynamic effects under laser irradiation (Wang and Niu 2021; Lange et al. 2021). We employed the commonly used IR780 dye (Wang and Niu 2021) to generate OMV-IR780 complexes to explore the photo-therapeutic potential as a proof-of-concept. We first investigated the photothermal performance of OMV-IR780 under a 780 nm continuous wave (CW) laser at a power density of 1.0 W/cm^2 for up to 10 min. Figure 4a, b and Additional file 1: Fig. S5 shows that OMV-IR780 underwent a significant temperature change (~ 21 °C) starting at 1 min, with no differences observed in the control. Such a considerable temperature increase is sufficient to induce hyperthermia damage as part of cancer therapy
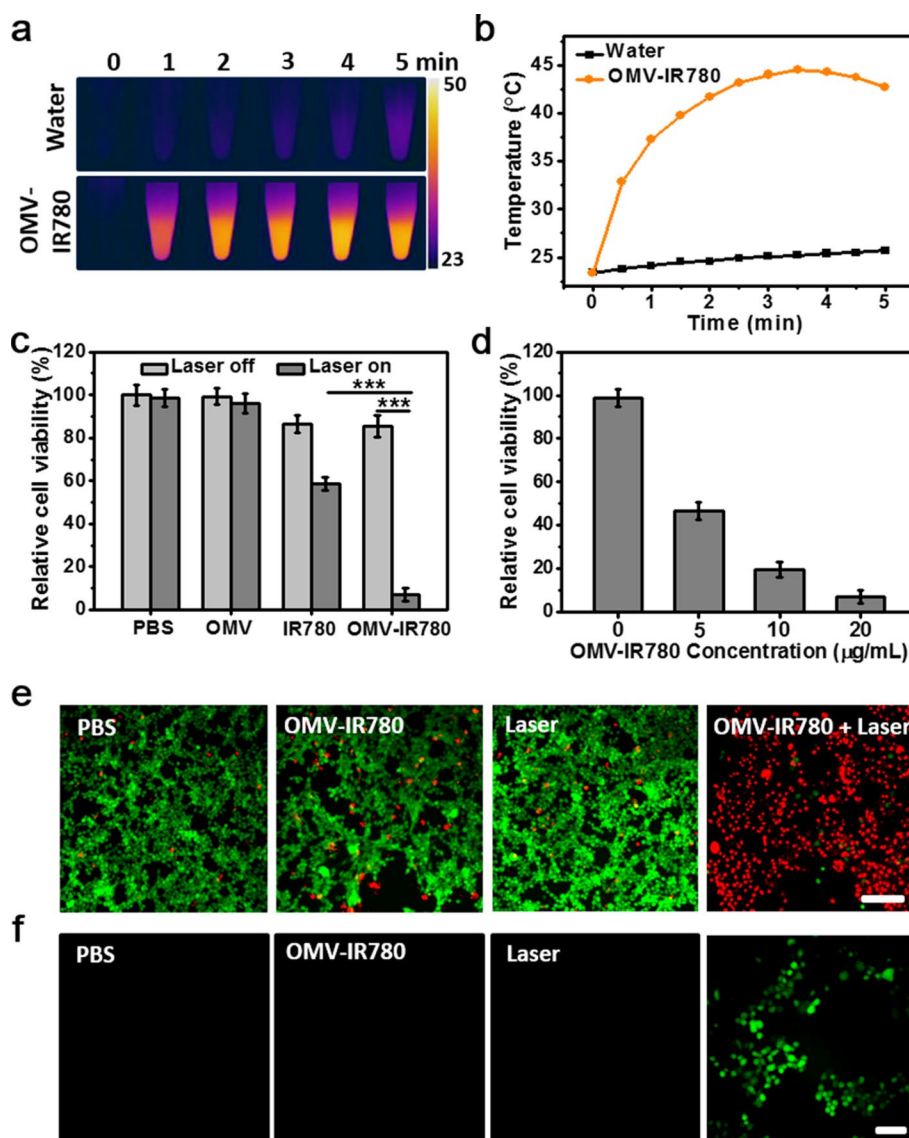
Fig. 4 In vitro phototherapy with OMV-IR780. **a**, **b** Thermal images and temperature change curves of OMV-IR780 and OMV upon exposure to a 780 nm CW laser (1 W/cm²). **c** Relative viabilities of 4T1 cells after treatment with PBS, OMV (~ 20 μg), IR780 (1.6 μg/mL) or OMV-IR780 complex (~ 20 μg) with or without 780 nm CW laser irradiation at 1 W/cm² for 5 min. **d** Relative viabilities of 4T1 cells after treatment with OMV-IR780 at different concentrations with 780 nm CW laser irradiation at 1 W/cm² for 5 min. **e** Fluorescence images of live/dead staining of 4T1 cells after different treatments. Red color: dead cells; green color: live cells. Scale bar, 100 μm. **f** Fluorescence images of ROS generation in 4T1 cells after different treatments. Scale bar, 100 μm

(Liu et al. 2021a, b, c). We also assessed the photodynamic profile of OMV-IR780 by 1,3-diphenylisobenzofuran (DPBF) (Liu et al. 2020). Additional file 1: Fig. S6 shows a significant decrease of DPBF absorption intensity in OMV-IR780 samples after laser irradiation, indicating the generation of reactive oxygen species (ROS) and a successful photodynamic effect.

We next assessed the phototherapy effect of OMV-IR780 by measuring 4T1 cell viability with a standard MTT assay. Empty OMV and OMV-IR780 were incubated with 4T1

cells for 6 h and then irradiated by a 780 nm CW laser at different laser power. Figure 4c displays that OMV led to negligible cytotoxicity while OMV-IR780 led to remarkable cell ablation under 1.0 W/cm^2 laser irradiation than free IR780. Additionally, we also explored different OMV-IR780 concentrations on cell phototherapy. Figure 4d shows that the toxicity of OMV-IR780 to cancer cells under laser irradiation was correlated with OMV-IR780 concentration, with the highest concentration (20 µg/mL) having the strongest cytotoxic effect. To visually observe the phototherapy effect of OMV-IR780 in 4T1 cells, calcein-acetoxymethyl (calcein-AM) and ethidium homodimer-1 (EthD-1) were used to co-stain live and dead cells, respectively. As observed in Fig. 4e, 4T1 cells incubated with OMV-IR780 displayed strong photo-cytotoxicity, with minimal signs of damage in the control groups. To further explore whether some of this phototoxicity originated from photodynamic effects, we used non-fluorescent 2′,7′-dichlorodihydrofluorescein diacetate (H2DCFDA) as a ROS sensor, which emits green fluorescence upon ROS detection. Figure 4f and Additional file 1: Fig S7 shows that strong green fluorescence was generated when OMV-IR780 treated cells were irradiated, but not in the other 3 control groups.

In vivo phototherapy of tumors using OMV-IR780

Given the promising photothermal and photodynamic effect of OMV-IR780 on cell ablation, we set out to test if it can also be used for phototherapy in vivo. For this, 4T1 tumor-bearing mice were randomly divided into six groups (n = 5 each) receiving one of the following treatments: (i) PBS, (ii) PBS + laser, (iii) OMV, (iv) OMV + laser, (v) OMV-IR780, (vi) OMV-IR780 + laser. The irradiation time was chosen at 6 h post-injection based on the in vivo MSOT imaging results. The temperature changes of tumor areas were recorded by a thermal imaging camera for 10 min. As shown in Fig. 5a, b, under laser irradiation, the tumor temperature in animals treated with OMV-IR780 increased to 50 °C, while the control groups treated with PBS or OMV only reached 39.7 °C and 40.2 °C, respectively. Subsequently, we monitored all animals' tumor volumes and body weights daily for 7 days. The mice treated with OMV-IR780 + laser demonstrated almost complete tumor elimination. In comparison, the tumors from the other 5 control groups continued to grow rapidly, up to 600 mm^3 on day 7 (Fig. 5c, d). This result indicates that OMV-IR780 can be efficiently used for phototherapy and tumor suppression. Furthermore, the therapeutic effect on tumors was confirmed by staining tumor slices with hematoxylin and eosin (H&E) 7 days after treatment. The tumor slices from OMV-IR780 + laser-treated mice showed severe necrosis due to the phototherapeutic effect, while the other control groups displayed a high number of abnormal cells with typical cancerous features (Fig. 5f). Additionally, the biosafety of OMV-IR780 was evaluated by body weight monitoring and H&E staining of major organs. The body weight from of all the animals showed a normal variation during the observation period, suggesting the absence of any serious side effects (Fig. 5e). H&E staining of vital organs revealed no pathological tissue damage such as cellular shrinkage, nucleus fragmentation, or necrosis that might indicate phototoxicity or bioincompatibility of OMV-IR780 (Additonal file 1: Fig. S8). Overall, these results indicate that OMV-IR780 can enable excellent phototherapy of tumors without any major signs of toxicity.
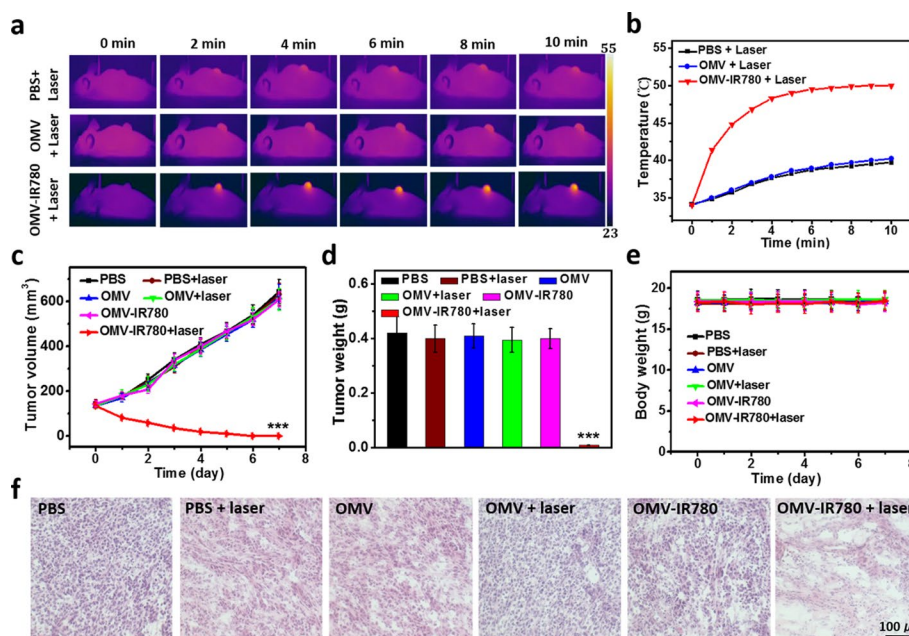
Fig. 5 In vivo phototherapy with OMV-IR780. **a** Infrared thermal images of representative 4T1 tumor-bearing mice after different treatments exposed to a 780 nm laser (1 W/cm^2) recorded at different time intervals (n = 5 per group). **b** Temperature of tumors in different treatment groups monitored by a thermal infrared camera upon laser irradiation as indicated in the panel-a. **c**–**e** After the indicated treatments, the relative tumor volumes, tumor weight, and the body weight of mice. **f** H&E staining of tumors isolated from mice at day 7 after the indicated treatment

Discussion

Here we developed OMVs as nanocarriers of cationic dyes for optoacoustic image-guided phototherapy. Because of electrostatic and hydrophobic interactions, hydrophobic cationic dyes (IR780, Cy7, Cy7.5) can tightly bond with OMVs lipid components and surface, ensuring a high loading efficiency. The formed nanosized OMV-Dye complexes are highly stable in aqueous conditions and generate strong optoacoustic signals. Due to an enhanced permeability and retention effect, these OMV-Dye complexes display remarkable tumor accumulation, enabling sensitive tumor detection using optoacoustic imaging. As a proof-of-concept, we generated OMV-IR780 complexes and demonstrated a superior phototherapy effect on tumor elimination with minimal toxicity in a mouse tumor model.

A variety of nano-formulations (e.g. liposome, micelle, albumin) have been reported to package cationic dyes to enhance stability and bioavailability based on their lipophilic property (Wang and Niu 2021). For example, heparin–folic acid conjugate (Yue et al. 2013), solid lipid nanoparticles (Kuang et al. 2017), and transferrin (Wang et al. 2016) have been used to load IR780. In addition, intrinsically self-assembled nanoparticles have been recently introduced by conjugating polyethylene glycol with the hydrophobic IR780, which can form a robust and water-soluble nanostructure (Yuan et al. 2015). Most synthetic agents must be chemically modified or conjugated to develop effective nanoformulations for in vivo applications. In contrast, OMVs are natural, preformed membrane vesicles, with rigid and stable membrane structures (Gujrati et al. 2019; Gujrati 2014). Importantly, OMVs are generated from low pathogenic laboratory strains

Liu *et al. Cancer Nanotechnology*   (2023) 14:36

Page 9 of 14

of bacteria, and they have been used to deliver diverse cargos including genes, proteins, drugs, and biopolymers for cancer therapy (Li and Liu 2020; Gujrati et al. 2014, 2019, 2016; Li et al. 2020). Further, the presence of LPS on the OMVs provides the negative charge necessary for binding cationic molecules (He et al. 2019). Therefore, by utilizing both electrostatic and hydrophobic interactions, OMV-Dye complexes can be generated via simple co-incubation approach.

Nanocarriers loaded with NIR-absorbing dyes can be used for photo-theranostics of tumors because these agents can utilize light to generate optical or ultrasound signals for diagnosis while simultaneously generating heat or ROS for tumor elimination (Liu et al. 2021a, b, c; Liu et al. 2019a, b). The NIR-absorbing dyes that we formulated as OMV-dye complexes (IR780, Cy7, Cy7.5) show good NIR absorption and stability in aqueous conditions, and could thus be used for NIR light-excited optoacoustic imaging and phototherapy. Optoacoustic technology can provide more information from deep tissue with high contrast and spatial resolution compared to fluorescence (Ntziachristos and Razansky 2010; Gujrati et al. 2017; Liu et al. 2021a, b, c; Liu et al. 2022a, b; Liu et al. 2022a, b). In this study, optoacoustic imaging in phantoms and in vivo tumor models using OMV-Dyes revealed strong optoacoustic signals and precise tumor detection. Moreover, in our pilot study we clearly demonstrated that OMV-IR780 can be used as a phototherapy agent to achieve tumor suppression in vivo. Here, the excitation energy can be released as nonradiative decay in the form of heat, while also promoting a singlet to triplet state electron transition in the form of ROS generation (Feng et al. 2020).

In addition, hyperthermia increases blood flow, which could lead to increased immune cell infiltration. As OMVs are known to affect immunomodulations, they could contribute to anti-tumor responses in mice (Gujrati et al. 2014; Chen et al. 2020; Kim et al. 2017). Therefore, when used as photo-theranostic agents, OMV-Dyes may exert synergistic immunomodulatory functions. Lastly, OMVs are biodegradable nanostructures that degrade in the cellular lysosomes within 48–72 h (Gujrati and Jon 2014). Upon OMVs degradation, the released free dyes might remain in the tumor area,undergo clearance, or potentially accumulating in other organs. However, as we illuminated tumors locally in the phototherapy experiments, there was no potential for phototoxicity within vital organs.

In summary, cationic dye-bonded OMVs were generated and used for optoacoustics-guided phototherapy of tumors. The formed OMV-Dyes can be synthesized by a facile procedure. The light-excitable OMV-Dyes not only offer strong optoacoustic signals for tumor detection, but also induce an efficient therapeutic effect for tumor elimination in vivo. We propose that OMVs can function as biocompatible nanocarriers to efficiently deliver cationic molecules for tumor theranostics applications.

Experimental section

Materials

Bacterial OMVs were produced according to our previously established protocol (Gujrati et al. 2014, 2019). Briefly, bacteria were cultured in 1.5-L flasks at 30 °C and 180 rpm. Bacterial cells were removed by centrifugation at $7500 \times g$ for 45 min at 4 °C. The resulting supernatant was filtered (0.45-µm membrane filter—Nalgene, Thermo Scientific), and concentrated to 100 mL using a 100-K ultrafiltration

membrane. OMVs were precipitated by treating the concentrate with ammonium sulphate (at final concentration, 400 g L^{-1}) at 4 °C overnight. Crude OMVs were obtained by centrifugation at 12,000 × g for 60 min. The resulting OMV pellet was separated from other impurities using a sucrose gradient (1 mL each of 2.5, 1.6 and 0.6 M sucrose) based ultracentrifugation at 150,000 × g for 3–5 h at 4 °C. The collected OMV fractions were washed with PBS and then centrifuged at 150,000 × g for 2 h at 4 °C followed by resuspension of the pellet in 1 mL PBS containing 15% glycerol for storage at − 20 °C until use. Total protein concentration was estimated using the bicinchoninic acid (BCA) assay (Thermo Scientific), and this was defined to be the OMV concentration.

IR780 iodine, indocyanine green (ICG), 2′,7′-dichlorodihydrofluorescein diacetate (H2DCFDA), 1,3-diphenylisobenzofuran (DPBF), 3-(4,5-dimethylthiazol-2-yl)-2,5-diphenyltetrazolium bromide (MTT) were purchased from Sigma-Aldrich. Cyanine7 amine(Cy7) and cyanine7.5 amine (Cy7.5) were bought from Lumiprobe Gmbh. CR780 was previously obtained (Liu et al. 2021a, b, c). Calcein-acetoxymethyl (AM) and ethidium homodimer-1 (EthD1) were bought from Thermo Fisher Scientific.

Formulation of OMV-Dyes (IR780, Cy7, Cy7.5)

OMVs (100 µg in 1 mL PBS) and 10 µL cationic dyes (IR780, Cy7, Cy7.5) (7 mg/mL) were mixed together by shaking in an incubator for 1 h. Then the OMV-Dye complexes were obtained by centrifugation at 45 000 rpm at 4 °C for 1 h (Gujrati et al. 2014). Free dye was removed by washing pellets five times by resuspending in 1 mL PBS between centrifugation steps as mentioned above. The obtained OMV-Dyes were stored at 4° until further use. In addition, a control containing only free dye in PBS was subjected to similar conditions of repeated centrifugation and washing.

Characterization of OMV-Dyes

The morphologies of OMVs were measured by transmission electron microscopy (Zeiss Libra 120 Plus, Carl Zeiss NTSb GmbH, Oberkochen, Germany). The lipophilicity of the dyes was determined by using the octanol–water partition coefficient (log *P*) as described before (Oba et al. 2012). The particle size and zeta potential were measured by Malvern Zetasizer. The absorption spectra of OMV-Dyes were measured with a UV-1800 spectrometer (Shimadzu, Japan). The dye loading efficiency was also determined by UV-1800 spectrometer using the dye standard curve. Optoacoustic spectra of samples were obtained out using an MSOT inVision 256-TF (iThera Medical, Munich, Germany) and the spectral correction was performed with Indian ink (Fuenzalida Werner et al. 2020). For optoacoustic evaluation, samples were placed in a cylindrical tissue-mimicking agar phantom and scanned using MSOT (Gujrati et al. 2019). Briefly, the cylindrical phantom contained 1.3% (w/w) agar (Sigma-Aldrich, St. Louis, MO, USA) to provide solidity and 6% (v/v) intralipid emulsion (20%, Sigma-Aldrich) for light diffusion to enable uniform illumination of the sample. The samples were placed in the tissue-mimicking agar phantom using a plastic tube that had a diameter of 3 mm. MSOT data were acquired approximately from the middle of the phantom.

In vivo optoacoustic imaging

All procedures involving animal experiments were approved by the Government of Upper Bavaria. The 4T1 tumor models were constructed by implanting 4T1 cells (1×10^6) on the backs of 6 weeks old AthymicNude-Fox1nu mice. In vivo optoacoustic imaging and phototherapy studies were carried out when the tumor size reached $\sim$100 mm^3. 4T1 tumor-bearing mice (n=5) per treatment were i.v. injected with 100 μL ($\sim$100 μg OMVs or OMV-Dye) of OMV-IR780, OMV-Cy7, and OMV-Cy7.5. In vivo optoacoustic images were acquired at different time points (0, 6, 24 h) using an MSOT inVision 256-TF (iThera Medical, Munich, Germany). After 24 h, the treated mice were sacrificed, and the major organs and tumors were isolated for ex vivo MSOT scanning. The averaged optoacoustic signals of tumors and major organs were extracted using ViewMSOT 4.0 software (iThera Medical, Munich).

Evaluation of the photothermal and photodynamic activity of OMV-IR780

The photothermal conversion abilities of OMV and OMV-IR780 were evaluated in phantoms by recording their temperature changes under exposure to a 780 nm CW laser (1 W/cm^2) for 5 min using an infrared thermal camera. The photodynamic effect of OMV-780 was determined by DBPF, which has a decreased absorption when encountering ROS (Liu et al. 2020). Briefly, a mixed solution containing OMV-IR780 and DBPF was measured with the absorption spectrum before and after 1 min irradiation with a 780 nm CW laser, and then checked for absorption intensity changes.

In vitro phototherapy

4T1 cells (1×10^4 per well) were subcultured in a 96-well plate overnight. The cells were incubated with OMVs ($\sim$20 μg) or different concentrations of OMV-IR780 ($\sim$5,10, or 20 μg for 6 h, followed by laser irradiation (780 nm CW laser) for 5 min. Then the cells were cultured for another 24 h to calculate the relative cell viabilities by MTT assay. The live/dead cells were visualized by the staining of Calcein-AM and EthD1. Briefly, the 4T1 cells were seeded in 96-well plates and subjected to different treatments. After 24 h, the cells were co-stained with Calcein-AM and EthD1 for 30 min and then imaged with a Leica DMI3000 B Inverted Microscope (Wetzlar, Germany). In vitro photodynamic effect was identified by H2DCFDA, which emits green fluorescence in the presence of ROS. Pre-seeded 4T1 cells were co-incubated with H2DCFDA and PBS or OMV-IR780 for 6 h, which was then replaced with fresh medium. The cells were irradiated by a 780 nm CW laser (1 W/cm^2) for 5 min and then imaged by the Leica DMI3000 B Inverted Microscope.

In vivo phototherapy

The tumor-bearing mice were randomly divided into 6 groups (n=5 per group) and given different treatments as follows: (i) PBS, (ii) PBS+laser, (iii) OMV, (iv) OMV+laser, (v) OMV-IR780, (vi) OMV-IR780+laser (100 μL, $\sim$100 μg OMVs or OMV-Dye). The laser irradiation was operated with 1 W/cm^2 for 10 min. The thermal images and tumor temperature from each group were recorded by an infrared thermal camera. The tumor volume

Liu *et al. Cancer Nanotechnology*   (2023) 14:36

Page 12 of 14

and body weight were measured until day 7, after which the mice were sacrificed and the tumors and major organs from each group were isolated for hematoxylin–eosin (H&E) staining.

Statistics

Statistical analyses were performed using OriginPro 8 (Northampton, Massachusetts, USA). Inter-group differences were assessed for significance using the paired *t*-test. Results were expressed as mean $\pm$ SD, and differences were considered significant if $p < 0.05$.

Supplementary Information

The online version contains supplementary material available at https://doi.org/10.1186/s12645-023-00191-w.

Additional file 1: Figure S1. Chemical structures of cationic and anionic dyes used in the study. **Figure S2.** Optoacoustic signal intensity of OMV-Dyes at different concentrations. **Figure S3.** Representative unmixed MSOT images of a 4T1 subcutaneous tumor mouse model intravenously injected with OMV (~100µg) or IR780 free dye. **Figure S4.** The biodistribution of OMV-IR780, OMV-Cy7, and OMV-Cy7.5 in vital organs 24 h after intravenous injection into 4T1 tumor-bearing mice. Animals were injected with ~100µg of OMV-IR780, OMV-Cy7, and OMV-Cy7.5. (a) Optoacoustic coronal plane images of major organs. (b) Optoacoustic signal intensity of major organs. **Figure S5.** Temperature change curves of OMV-IR780 upon exposure to a 780 nm CW laser (1 W/cm^2). **Figure S6.** Degradation of DPBF in the presence of OMV-IR780 before and after laser irradiation. **Figure S7.** (a) Quantitative fluorescence intensities of AM/PI images in different treated groups for Figure 4e. (b) Quantitative fluorescence intensities of ROS generation in 4T1 cells after different treatments for Figure 4f. **Figure S8.** Representative H&E staining of vital organs after the indicated treatments.

Declarations

Ethics approval and consent to participate

All procedures involving animal experiments were approved by the Animal Care and Handling Office of Helmholtz Zentrum München and Government of Upper Bavaria.

Consent for publication

All authors consent for publication.

Competing interests

VN is an equity owner and consultant at iThera Medical GmbH, member of the Scientific Advisory Board at SurgVision BV / Bracco Sp.A, owner at Spear UG, founder and consultant at I3, and founder of Sthesis. The remaining authors declare no competing interests.

Data Availability

All data presented in the paper are available from the authors upon reasonable request.

References

Avila-Calderón ED, Ruiz-Palma MdS, Aguilera-Arreola MG et al (2021) Outer membrane vesicles of gram-negative bacteria: an outlook on biogenesis. Front Microbiol 12:557902

Beziere N, Lozano N, Nunes A et al (2015) Dynamic imaging of PEGylated indocyanine green (ICG) liposomes within the tumor microenvironment using multi-spectral optoacoustic tomography (MSOT). Biomaterials 37:415–424

Cai Y, Si W, Huang W et al (2018) Organic dye based nanoparticles for cancer phototheranostics. Small 14(25):1704247

Chen Q, Bai H, Wu W et al (2020) Bioengineering bacterial vesicle-coated polymeric nanomedicine for enhanced cancer immunotherapy and metastasis prevention. Nano Lett. 20(1):11–21

Feng G, Zhang GQ, Ding D (2020) Design of superior phototheranostic agents guided by Jablonski diagrams. Chem Soc Rev 49(22):8179–8234

Fuenzalida Werner JP, Huang Y, Mishra K et al (2020) Challenging a preconception: optoacoustic spectrum differs from the optical absorption spectrum of proteins and dyes for molecular imaging. Anal Chem 92(15):10717–10724

Furuyama N, Sircili MP (2021) Outer membrane vesicles (OMVs) produced by gram-negative bacteria: structure, functions, biogenesis, and vaccine application. Biomed Res Int 2021:1490732–1490732

George S, Hamblin MR, Kishen A (2009) Uptake pathways of anionic and cationic photosensitizers into bacteria. Photochem Photobiol Sci 8(6):788–795

Gujrati V, Jon S (2014) Bioengineered bacterial outer membrane vesicles: what is their potential in cancer therapy? Nanomedicine 9(7):933–935

Gujrati V, Kim S, Kim SH et al (2014) Bioengineered bacterial outer membrane vesicles as cell-specific drug-delivery vehicles for cancer therapy. ACS Nano 8(2):1525–1537

Gujrati V, Lee M, Ko YJ et al (2016) (2016) Bioengineered yeast-derived vacuoles with enhanced tissue-penetrating ability for targeted cancer therapy. Proc Natl Acad Sci 113:710

Gujrati V, Mishra A, Ntziachristos V (2017) Molecular imaging probes for multi-spectral optoacoustic tomography. Chem Commun 53(34):4653–4672

Gujrati V, Prakash J, Malekzadeh-Najafabadi J et al (2019) Bioengineered bacterial vesicles as biological nano-heaters for optoacoustic imaging. Nat Commun 10:1114

He P, Zhang E, Qi R et al (2019) Application of cationic conjugated polymer-outer membrane vesicle complexes in inhibiting red blood cell aggregation. Org Mater 1(01):038–042

Jiang C, Cheng H, Yuan A et al (2015) Hydrophobic IR780 encapsulated in biodegradable human serum albumin nanoparticles for photothermal and photodynamic therapy. Acta Biomater 14:61–69

Kim OY, Park HT, Dinh NTH et al (2017) Bacterial outer membrane vesicles suppress tumor by interferon-gamma-mediated antitumor response. Nat Commun 8:626

Kotras C, Fossépré M, Roger M et al (2019) A cationic tetraphenylethene as a light-up supramolecular probe for DNA G-quadruplexes. Front Chem 7:493

Kuang Y, Zhang K, Cao Y et al (2017) Hydrophobic IR-780 dye encapsulated in cRGD-conjugated solid lipid nanoparticles for nir imaging-guided photothermal therapy. ACS Appl Mater Interfaces 9(14):12217–12226

Lange N, Szlasa W, Saczko J et al (2021) Potential of cyanine derived dyes in photodynamic therapy. Pharmaceutics 13(6):818

Leriche G, Stengel D, Onofrei D et al (2019) Fusion of bipolar tetraether lipid membranes without enhanced leakage of small molecules. Sci Rep 9:19519

Li R, Liu Q (2020) Engineered bacterial outer membrane vesicles as multifunctional delivery platforms. Front Mater 7:202

Li K, Zhang Y-Y, Jiang G-Y et al (2015) A bivalent cationic dye enabling selective photo-inactivation against Gram-negative bacteria. Chem Comm 51(37):7923–7926

Li Y, Zhao R, Cheng K et al (2020) Bacterial outer membrane vesicles presenting programmed death 1 for improved cancer immunotherapy via immune activation and checkpoint inhibition. ACS Nano 14(12):16698–16711

Li C, Liu C, Fan Y et al (2021) Recent development of near-infrared photoacoustic probes based on small-molecule organic dye. RSC Chem Biol 2(3):743–758

Liu Y, Teng L, Liu HW et al (2019a) Recent advances in organic-dye-based photoacoustic probes for biosensing and bioimaging. Sci China Chem 62(10):1275–1285

Liu Y, Bhattarai P, Dai Z, Chen X (2019b) Photothermal therapy and photoacoustic imaging via nanotheranostics in fighting cancer. Chem Soc Rev 48(7):2053–2108

Liu Z, Cao T, Xue Y et al (2020) Self-amplified photodynamic therapy through the (1) O(2) -mediated internalization of photosensitizers from a ppa-bearing block copolymer. Angew Chem Int Ed 132(9):3740–3746

Liu N, Gujrati V, Malekzadeh-Najafabadi J et al (2021a) Croconaine-based nanoparticles enable efficient optoacoustic imaging of murine brain tumors. Photoacoustics 22:100263

Liu N, O'Connor P, Gujrati V et al (2021b) Facile synthesis of a croconaine-based nanoformulation for optoacoustic imaging and photothermal therapy. Adv Healthc Mater 10(9):2002115

Liu N, Chen X, Kimm MA et al (2021c) In vivo optical molecular imaging of inflammation and immunity. J Mol Med 99(10):1385–1398

Liu N, Mishra K, Stiel AC et al (2022a) The sound of drug delivery: optoacoustic imaging in pharmacology. Adv Drug Deliv Rev 189:114506

Liu N, O'Connor P, Gujrati V et al (2022b) Multifunctional croconaine nanoparticles for efficient optoacoustic imaging of deep tumors and photothermal therapy. Nanophotonics. https://doi.org/10.1515/nanoph-2022-0469

Ntziachristos V, Razansky D (2010) Molecular imaging by means of multispectral optoacoustic tomography (MSOT). Chem Rev 110(5):2783–2794

Nunes A, Pansare VJ, Beziere N et al (2018) Quenched hexacene optoacoustic nanoparticles. J Mater Chem B 6(1):44–55

Oba Y, Poulson SR (2012) Octanol-water partition coefficients (Kow) vs pH for fluorescent dye tracers (fluorescein, eosin Y), and implications for hydrologic tracer tests. Geochem J 46(6):517–520

Qing G, Gong N, Chen X et al (2019) Natural and engineered bacterial outer membrane vesicles. Biophys Rep 5(4):184–198

Schwechheimer C, Kuehn MJ (2015) Outer-membrane vesicles from gram-negative bacteria: biogenesis and functions. Nat Rev Microbiol 13:605–619

Svechkarev D, Mohs AM (2019) Organic fluorescent dye-based nanomaterials: advances in the rational design for imaging and sensing applications. Curr Med Chem 26(21):4042–4064

Wang L, Niu C (2021) IR780-based nanomaterials for cancer imaging and therapy. J Mater Chem B 9(20):4079–4097

Wang K, Zhang Y, Wang J et al (2016) Self-assembled IR780-loaded transferrin nanoparticles as an imaging, targeting and PDT/PTT agent for cancer therapy. Sci Rep 6:27421

Yuan A, Qiu X, Tang X et al (2015) Self-assembled PEG-IR-780-C13 micelle as a targeting, safe and highly-effective photothermal agent for in vivo imaging and cancer therapy. Biomaterials 51:184–193

Yue C, Liu P, Zheng M et al (2013) IR-780 dye loaded tumor targeting theranostic nanoparticles for NIR imaging and photothermal therapy. Biomaterials 34:6853–6861

Publisher's Note